Fuel 390 (2025) 134723

Contents lists available at ScienceDirect

Fuel

journal homepage: www.elsevier.com/locate/fuel

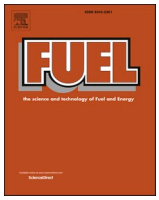

Full Length Article

Comparative analysis and optimization of performance of air-breathing and conventional PEM fuel cells

Faseeh Abdulrahman [a], Mohammed S. Ismail [b,*], S. Mani Sarathy [a]

[a] Clean Energy Research Platform, Physical Sciences and Engineering (PSE) Division, King Abdullah University of Science and Technology (KAUST), Thuwal 23955-6900, Saudi Arabia
[b] School of Engineering, University of Hull, Hull HU6 7RX, United Kingdom

ARTICLE INFO

Keywords:
Air-breathing PEMFC
Conventional PEMFC
Numerical modelling
Taguchi analysis

ABSTRACT

Polymer electrolyte membrane fuel cells (PEMFCs) are a critical part of the energy transition as they can be sustainably powered by hydrogen fuel. They have gained significant attention recently due to their compact design and simplified system, which makes them ideal for portable applications. This paper presents a first-of-its-kind comparative study of air-breathing and conventional PEMFCs, conducted using a combined approach of numerical modelling and Taguchi analysis. A comprehensive multiphysics one-dimensional model was developed for each type of fuel cell. The results show that the conventional fuel cell outperforms the air-breathing fuel cell, especially at high current densities. This is due to its significantly higher mass and heat transfer coefficients on the cathode side of the conventional fuel cell, which also enhances its heat dissipation. Taguchi analysis ranked specific design parameters by their impact on fuel cell performance, identifying cathode GDL thickness as the most influential. The results of the parametric study using numerical models confirm this ranking and the significance of the factors proposed by Taguchi analysis. Interestingly, the performance of air-breathing PEMFCs is more sensitive to cathode GDL porosity compared to conventional PEMFCs. This increased sensitivity is primarily due to higher diffusion limitations and a lower oxygen mass transport coefficient in air-breathing PEMFCs.

1. Introduction

World energy consumption is increasing rapidly every year with population growth and economic development. According to the U.S. Energy Information Administration (EIA), in the International Energy Outlook 2021, global energy use will rise by half by 2050 with no significant policy or technological developments [1]. Concurrently, global electricity demand is forecasted to at least double from 25,000 TWh to 52000–71000 TWh by 2050 [2], thus putting the need for sustainable energy solutions at a high level to meet future requirements. The major share of the energy is generated from fossil fuels; however, interest is rising towards renewable sources of energy and increasing energy efficiency since these sources can help minimize the potential adverse impacts on the environment and human health while fulfilling the growing demands for energy.

Fossil fuel combustion releases a wide range of pollutants, including toxins and greenhouse gases that are harmful to ecosystems and human health. Such discharges are major drivers of air pollution and global climate change. This makes hydrogen a more attractive option than the other alternatives because it is a cleaner form of energy that emits no by-products except water vapor when it burns. Besides, hydrogen can be produced from water electrolysis driven by clean electricity generated from renewable energy sources such as wind and solar energy.

PEMFCs will be critical in driving the hydrogen economy forward since they have a low operational temperature, high efficiency, and rapid startup [3–7]. These characteristics make them a potential replacement for several traditional conversion technologies used in automotive, portable, and stationary applications. Notably, air-breathing PEMFCs have recently attracted attention because they can be used to power small portable electronic devices such as smartphones and laptops, thereby providing relatively long operation and grid-independent energy solutions. However, the PEMFC technology is currently too expensive to be adapted for consumer devices [8,9]. Sapkota et al. [10] discussed the potential of planar PEMFCs for powering portable devices from hydrogen, highlighting advancements in thin, flexible designs that are critical for their deployment.

The air-breathing PEMFC extracts oxygen from the ambient and relies on natural convection for heat and water exchange with the

* Corresponding author.
E-mail addresses: faseeh.kulangarakandiyil@kaust.edu.sa (F. Abdulrahman), m.s.ismail@hull.ac.uk (M.S. Ismail), mani.sarathy@kaust.edu.sa (S.M. Sarathy).

https://doi.org/10.1016/j.fuel.2025.134723
Received 18 November 2024; Received in revised form 9 February 2025; Accepted 12 February 2025
Available online 19 February 2025

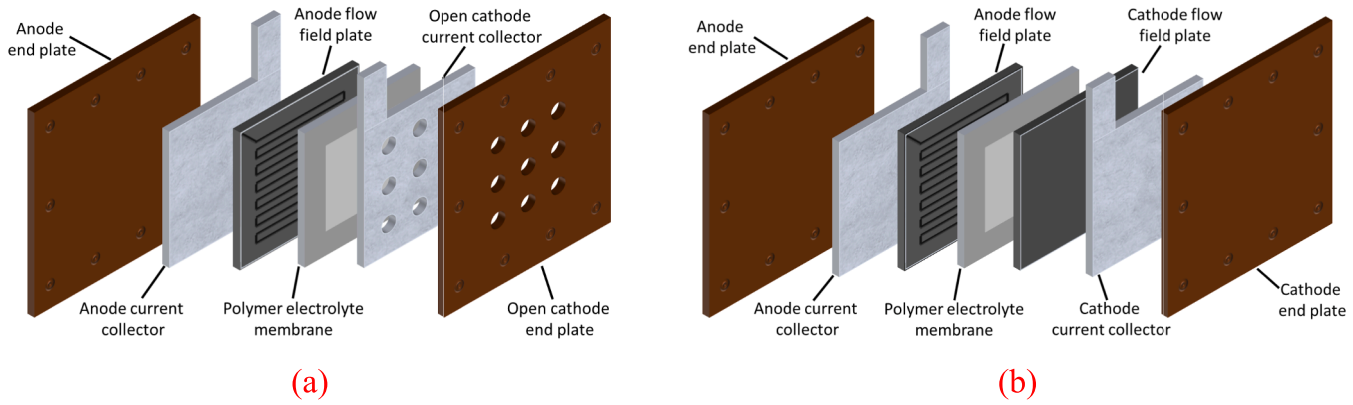

Fig. 1. Schematic diagrams of (a) air-breathing and (b) conventional PEMFCs.

ambient, thus eliminating the subsystems for oxygen/air supply, humidification and cooling and simplifying the fuel cell system. Compared to the conventional PEMFCs, which typically rely on an active system to supply oxygen and exchange heat and water, air-breathing PEMFC systems are significantly smaller and more appropriate for portable applications [11]. However, in air-breathing PEMFC, the heat and mass transfer coefficients associated with natural convection are relatively low, leading to lower performance compared to the conventional PEMFCs. This paper presents a comparative analysis of air-breathing and conventional PEMFCs, highlighting their respective advantages and limitations. It should be noted that conventional PEM fuel cells are typically cooled by liquids such as water or ethylene glycol, and as such, they are often referred to as liquid-cooled PEM fuel cells [12,13]. The key components of both the air-breathing and conventional types of PEMFC are shown in Fig. 1. Unlike the conventional PEMFC, which has a sealed cathode current collector, the air-breathing PEMFC features an open cathode current collector with perforations, allowing passive oxygen intake from the ambient environment. This eliminates the need for an external air supply system, simplifying the design and reducing system size.

Although Lithium ion batteries (LIB) have been widely adopted in portable electronics and electric vehicles because of their high energy density and efficiency [14–17], air-breathing PEMFCs have a number of distinct advantages [11,18,19]. Air-breathing PEMFCs provide higher energy densities of 500–1000 Wh/kg [20], way beyond current LIB technology with energy density value of 100–265 Wh/kg [15]. They also provide quick refueling, longer operation without major degradation, and only water as a by-product, thus offering a cleaner alternative to LIBs [21]. In addition, air-breathing PEMFCs can be scaled up easily from small portable devices to larger applications with high efficiency over a wide range of power output [22]. These features make air-breathing PEMFCs a very promising solution for portable power sources, especially in scenarios where extended operation and minimal downtime are required.

A number of studies have covered the conventional type of PEMFC, such as [23–33], but literature on air-breathing PEMFCs is very limited. Recent reviews have underlined that design optimizations play a crucial role in improving air-breathing PEMFC performance [19], and modelling studies have been very pivotal in understanding air-breathing PEMFC behavior [5,6,11,19,34–39]. Mathematical modelling offers a cost-effective and efficient way to optimize fuel cells including air-breathing PEMFCs, thus shortening the design cycles and saving cost and time. The following are the key findings of modelling studies conducted for air-breathing PEMFCs aimed at enhancing efficiency and understanding transport phenomena within these fuel cells.

Ismail et al. [40] developed a two-dimensional thermal model of an air-breathing PEMFC, which reveals that Joule heating contributed significantly to the heat transfer coefficient while operating at higher current densities, and dissipation is more effective with the cell orientation vertical or upwards-facing. Zhang et al. [41] developed a two-dimensional, non-isothermal, and multi-component numerical model of an air-breathing PEMFC. They found that cell performance improves with increasing temperature, anode flow rate, pressure, and relative humidity. They also demonstrated that cell orientation significantly affects local electrical current distributions. Another study by Zhang et al. [42] focused on optimization of the cell dimension, inter-cell spacing, and gap between the array and substrate showed improved stack performance. The temperature and species distributions in the study together with the flow patterns help to elucidate the coupled multi-physics phenomena.

Hwang [43] developed a three-dimensional model to analyze the species-electrochemical characteristics in a free-breathing planar fuel cell cathode and reported that staggered breathing hole arrangements performed better compared to the in-line arrangements. Wang et al. [44] created a three-dimensional model of an air-breathing PEMFC and provided a simplified equation for the dimensionless mass transfer coefficients needed for understanding oxygen transport limitations and fuel cell design optimization. The model's predictions have shown very good agreement with experimental results; therefore, it can provide real valuable insights into how the performance of air-breathing PEMFCs can be improved by coupling heat, mass transfer, and electrode dynamics. Kumar et al. [45] comparatively investigated two types of cathode designs for air-breathing PEMFCs: ducted and ribbed, by creating and running a three-dimensional, non-isothermal model. They found that the peak power density and limiting current density were higher with the ribbed cathodes. Another study by Kumar et al. [35], noted that the performance increases with larger width and depth of the channel, which is crucial for optimizing power density in portable hydrogen-powered devices.

Calili-Cankir et al. [46] developed a dynamic model of an air-breathing PEMFC to study the transient response to load changes. They found that with sudden changes to high loads, there exist optimal values for ambient temperature and GDL thickness that effectively mitigate overshoots and enhance steady-state performance. In another study, Calili-Cankir et al. [47] developed the dynamic model to compare the performances of air-breathing and conventional PEMFCs. The respective results showed that air-breathing cells exhibit slower dynamic responses and poorer heat dissipation, which impacts their performance under load changes. Another dynamic model for air-breathing PEMFCs was developed by Yalcinoz et al. [48] aiming to improve performance of air-breathing PEMFCs in real-world applications by addressing transient and steady-state behaviors. The key finding of the study is the validation of a dynamic model for an air-breathing PEMFC system as a reliable power source for portable applications.

Matamoros et al. [34] developed and run a non-isothermal, three-dimensional model to investigate the concentration and ohmic losses in

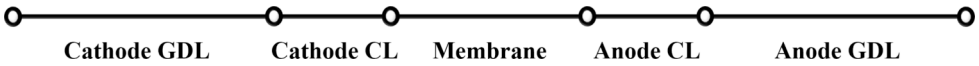

Fig. 2. Schematic diagram showing the one-dimensional PEMFC model and its main components.

free-breathing PEMFCs. They found that the most critical limiting factor is oxygen transport to active sites in the CL. Schmitz et al. [49] developed a two-dimensional isothermal model for a planar self-breathing PEMFC. They showed that the model can accurately predict the polarization curves and limiting current densities but noted problems caused by water condensation under broad ribs that impairs gas transport and hence performance. Additionally, dead-ended anode and cathode (DEAC) systems help achieve better gas utilization and reduce emissions [50]. Fan et al. [51] demonstrated a breakthrough in hydrogen and oxygen utilization through a DEAC system in a H_2-O_2 PEMFC stack, further advancing the efficiency and sustainability of PEMFC technology.

Ying et al. [52] developed a mathematical model that assessed the effects of various configurations in the cathode channel on the performance of air-breathing PEMFCs. The study showed that, compared to those in a forced convection environment, the concentration losses in a natural convection environment are higher. Ying et al. [53] has also developed a three-dimensional model of an air-breathing PEMFC, showing that natural convection has important performance effects, whereby the major limiting factor is the concentration losses, and there are great interactions in the way water distribution, temperature, velocity, and electrochemical reaction factors affect overall cell performance. In another study by Ying et al. [54], they found that a cathode channel width of 3 mm with an open ratio of around 75 % gives the best performance.

Fabian et al. [55] studied the effect of a broad range of ambient temperatures and relative humidities on a planar air-breathing hydrogen PEMFC and demonstrated that a peak power density of 356 mW/cm^2 is obtained at an ambient temperature of 20 °C and RH of 40 %. Williamson et al. [56] studied the dependence of temperature of a miniature air-breathing PEMFCs. They concluded that while higher temperature may bring about better performance at higher current densities as a result of enhanced air buoyancy, it can cause membrane dehydration at lower current densities. Al-Anazi et al. [57] tested an air-breathing PEMFC for harsh Saudi Arabian conditions and concluded that the peak performance occurs in summer and the output increases by 40 % with hydrogen humidification.

Yan et al. [58] developed a three-dimensional air-breathing PEMFC model and found that combining 50 % and 58.3 % cathode opening ratios in an air-breathing PEMFC stack significantly improved thermal management, leading to a more uniform temperature distribution and enhanced stack performance. Under assisted air-breathing conditions, the stack's performance increased by a factor of approximately 20 compared to natural convection, demonstrating a substantial boost in power output. Henriques et al. [59] developed a three-dimensional model of air-breathing PEMFC to study the effect of the geometry of the cathode channels on the air-breathing PEMFC performance. They found that redesigning the cathode flow channel geometry in a commercial portable PEMFC led to a significant efficiency improvement. Specifically, laboratory tests demonstrated that the new channel structure increased the fuel cell's efficiency by up to 26.4 %. Additionally, simulations revealed that using simpler, straight channels with adequate width not only improved performance but also reduced manufacturing costs. Matamoros et al. [60] developed a three-dimensional model and stated that shorter stacks improves the utilization of active areas, which is the most effective way to achieve efficient use of platinum in air-breathing configurations. Building on these findings, Shen et al. [61] investigated the transition from 2D to 3D flow channel designs in PEMFCs. Their study demonstrated that PEMFCs with 3D flow channels exhibited superior performance compared to those with parallel 2D flow channels, particularly at high current densities.

Recent studies have focused on optimizing the performance of PEMFCs by addressing key factors such as thermal management, mass transport, and system efficiency [62,63]. An increased GDL thickness can improve water retention, aiding membrane hydration and reducing the risk of reactant starvation over long-term operation; however, it may also lead to higher mass transport resistance, which could negatively impact performance [64,65]. Furthermore, material properties such as thermal conductivity enhance heat dissipation, while porosity and wettability play critical roles in hydrogen diffusion and water management, making them essential factors for optimizing PEMFC design [66].

Calili-Cankir et al. [11] conducted a comparative study of air-breathing and conventional PEMFCs using a mathematical model. They found that, unlike the conventional PEMFC, the air-breathing PEMFC performance was found to degrade with increasing porosity and decreasing cathode GDL thickness. This performance drop was attributed to the higher rate of water removal from the MEA, which led to membrane dehydration and increased ohmic losses. However, the model developed in [11] was zero-dimensional. In this study, we uniquely combine more accurate one-dimensional multiphysics modelling with Taguchi analysis for an extensive comparison of air-breathing and conventional PEMFCs. This innovative approach efficiently helps identify the critical design parameters that should be targeted to enhance the performance of each fuel cell type. These enhancements provide a deeper understanding of PEMFC behavior and contribute to the development of more efficient and reliable fuel cell systems, and further to progress on the scope beyond that is covered in the previous study.

2. Mathematical model

The mathematical model of the PEMFC developed in this study uses COMSOL Multiphysics and includes a microscale catalyst agglomerate model for the cathode electrode, which is more accurate than the classic homogeneous model [67,68]. Fig. 2 shows a schematic for the one-dimensional model considered in this study. It consists of all the key components of the fuel cell: the gas diffusion layers (GDLs), the catalyst layers (CLs) and the membrane. Although this one-dimensional model does not account for two- or three-dimensional effects, such as uneven oxygen distribution or localized heat dissipation, it is important to note that it captures the general trend (the focus of this study, which is not expected to change with higher-dimensional models) while remaining computationally efficient.

The equations presented are applicable to both conventional and air-breathing PEMFCs, with the major distinction being the boundary conditions used for the conservation equations of chemical species and energy. The model is based on the following assumptions [11,47,69]:

- Fuel cells operate in a steady-state, which is typically the standard operating condition for fuel cells.
- All the gases are assumed to be ideal as the fuel cell operates near room temperature and atmospheric pressure where deviations from ideality is small.
- Water is assumed to be present only in vapor form; this is due to increased heat generated and subsequently increased temperature within the membrane electrode assembly.
- Membrane is impermeable for gases, eliminating gas cross-over effect which remain minimal under normal conditions.
- The anode is in dead-end mode in the air-breathing PEMFC which is normally the case for this type of fuel cells.
- The only significant heat source is the reaction heat at the cathode CL, as it is considerably greater than other heat sources.

The following are the equations used for the models which were all taken from [11,67,68,70–72]. We will start with listing the governing conservation equations and then we will describe the auxiliary equations associated with these conservation equations. The mass is conserved by the following equation:

$$\nabla \bullet (\rho \vec{u}) = 0 \tag{1}$$

where $\vec{u}$ is the velocity vector and ρ is the density of the gaseous mixture. Below is the conservation equation of chemical species:

$$\rho(\vec{u} \bullet \nabla)\omega_i = -\nabla(j_i) + R_i \tag{2}$$

where ω_i is the mass fraction of species i, j_i is the mass flux relative to the mass averaged velocity of species i, and R_i is the source term representing the production or consumption rate. The charge is conserved by the following equation:

$$\nabla(-\sigma_s \nabla\phi_s) = \nabla \bullet I \tag{3}$$

$$\nabla(-\sigma_m \nabla\phi_m) = -\nabla \bullet I \tag{4}$$

where σ_s and ϕ_s are respectively the electrical conductivity and potential of the solid phase, and σ_m and ϕ_m are respectively the ionic conductivity and potential of the membrane phase, and I is the current density. The energy is conserved by:

$$\rho C_p(\vec{u}\cdot\nabla T) = \nabla\cdot(k\nabla T) + Q \tag{5}$$

where C_p is the specific heat capacity, k is the thermal conductivity, T is temperature and Q is the volumetric heat source term. j_i in Eq. (2) is defined as follows:

$$j_i = -\rho\omega_i \sum\nolimits_k D_{ik}^{eff} \frac{M}{M_k}\left(\nabla\omega_k + \omega_k \frac{\nabla M}{M}\right) \tag{6}$$

$$\rho = \frac{pM}{RT} \tag{7}$$

where p is the absolute pressure, M is the molecular weight of gas mixture, $D_{ik,eff}$ is the effective diffusivity coefficient of species i and k. $D_{ik,eff}$ is given by [71]:

$$D_{ik,eff} = \begin{cases} 0.008e^{4.81\varepsilon} D_{ik}, & \text{in the GDLs} \\ \varepsilon^{1.5} D_{ik}, & \text{in the CLs} \end{cases} \tag{8}$$

where ε is the porosity of GDL or CL. The source terms (R_i) of oxygen, water and hydrogen in Eq. (2) are given by:

$$R_{O_2} = -\frac{I_c}{4F} \tag{9}$$

$$R_{H_2O} = \frac{I_c}{2F} + nd\frac{I_c}{F} \tag{10}$$

$$R_{H_2} = -\frac{I_a}{2F} \tag{11}$$

where nd is the electro-osmotic drag, and F is the Faradays constant. The cathodic local volumetric current is, assuming spherical catalyst agglomerates, given by [68,73,74]:

$$I_c = 4F(1-\varepsilon_{cl})C_{O_{2,O}} \frac{r_{agg}{}^3}{(r_{agg} + \delta_{agg})^3}\left(\frac{1}{\xi k_c} + \frac{r_{agg}\,\delta_{agg}}{a_{agg}\,(r_{agg} + \delta_{agg})D_e}\right)^{-1} \tag{12}$$

where ξ is the effectiveness factor of the spherical agglomerate, r_{agg} is the radius of the agglomerate, a_{agg} is the specific surface area of agglomerate, D_e is the diffusivity of the dissolved oxygen in the ionomer, and δ_{agg} is the thickness of the ionomer film. $C_{O_{2,O}}$ is the oxygen concentration at the surface of the ionomer film:

$$C_{O_2} = \frac{C_{O_2,g}RT}{H_{O_2}} \tag{13}$$

where $C_{O_2,g}$ is the concentration of gaseous oxygen surrounding the agglomerate and H_{O_2} is the Henry's constant for oxygen in the ionomer phase. The specific surface area of spherical agglomerate is given by:

$$a_{agg} = \frac{3}{r_{agg}} \tag{14}$$

The effectiveness factor (ξ) is obtained using the following expressions:

$$\xi = \frac{1}{\phi}\left(\frac{1}{\tanh(3\phi)} - \frac{1}{3\phi}\right) \tag{15}$$

$$\phi = \frac{r_{agg}}{3}\sqrt{\frac{k_c/(1-\varepsilon_{cl})}{D_{O_2}}} \tag{16}$$

where ϕ is the Thiele modulus. k_c is the reaction rate constant:

$$k_c = \frac{a_{Pt}}{4F}\left(\frac{i_{o,c}}{c_{O_2,\mathrm{ref}}}\right)\exp\left(-\frac{\alpha_c F\eta_c}{RT}\right) \tag{17}$$

where, a_{Pt} is the specific surface area of the catalyst, $i_{o,c}$ is the exchange current density at cathode, $c_{O_2,\mathrm{ref}}$ is the reference concentration of the dissolved O_2, α_c is the charge transfer coefficient at cathode and η_c is the cathodic overpotential:

$$\eta_c = \phi_s - \phi_l - E_{eq} \tag{18}$$

where E_{eq} is the equilibrium (or reversible) voltage [11,67,68,70,71] and is given by:

$$E_{eq} = \frac{-\Delta H + T\Delta S}{2F} + \frac{RT}{2F}\ln\left(\frac{P_{H_2}\cdot P_{O_2}^{1/2}}{P_{H_2O}}\right) \tag{19}$$

where ΔH and ΔS are respectively the changes in enthalpy and entropy, and P_{H_2}, P_{O_2} and P_{H_2O} are respectively the partial pressures of H_2, O_2, and H_2O. a_{Pt} is given by:

$$a_{Pt} = \frac{m_{Pt}A_{Pt}}{\delta_{cl}} \tag{20}$$

where m_{Pt} is the platinum loading, A_{Pt} is the electrochemical active area of platinum particles, and δ_{cl} is the thickness of CL. The volumetric anodic current density, I_a, is given by:

$$I_a = \frac{i_{o,a}a_{Pt}RT}{H_{H_2}}\left(\frac{C_{H_2}}{C_{H_2,ref}}\right)\left(e^{\{-(1-\alpha_a)F/RT\}\eta_a} - e^{\{\alpha_a F/RT\}\eta_a}\right) \tag{21}$$

where, η_a is the anodic overpotential, $i_{o,a}$ is the exchange current density at the anode, H_{H_2} is the Henry's constant for H_2 in the ionomer phase, $C_{H_2,ref}$ is the reference concentration of H_2, α_a is the anodic charge transfer coefficient and η_a is the anodic overpotential:

$$\eta_a = \phi_s - \phi_l \tag{22}$$

The ionic conductivity of the membrane phase is given by:

$$\sigma_{\mathrm{mem}} = (0.514\lambda - 0.326)\exp\left[1268\left(\frac{1}{303} - \frac{1}{T}\right)\right] \tag{23}$$

where λ is the water content of the membrane phase and is defined as:

$$\lambda = \begin{cases} 0.043 + 17.81a - 39.85a^2 + 36a^3, & 0 < a \le 1 \\ 14 + 1.4(a-1), & 1 < a \le 3 \end{cases} \tag{24}$$

and a is the water activity and is given by:

Table 1
Physical parameters, dimensions, and constants used for the base cases of the models [11,67,68,75,76].

Parameters	Value
Gravitational acceleration,g	9.81 m/s^2
Universal gas constant,R	8.314 J/(mol.K)
Faraday's constant,F	96, 485 C/mol
Molecular weight of O_2, M_{O_2}	16g/mol
Molecular weight of H_2O, M_{H_2O}	18g/mol
Stephan-Boltzmann constant,σ_{Bolt}	5.67×10^{-8} W/(m^2.K^4)
Emissivity,e	0.90
Ambient temperature,T_∞	20° C
Ambient/cell pressure,P	1 atm
Oxygen/nitrogen molar ratio	21/79
Relative humidity,RH	0.5
Binary diffusivity of O_2 in air,$D_{O_2,\ air}$	2.79×10^{-5} m^2/s
Diffusivity of dissolved O_2 in ionomer,D_e	8.45×10^{-10} m^2/s
Binary diffusivity of O_2 and water vapour,D_{O_2,H_2O}	3.7×10^{-5} m^2/s
Binary diffusivity of O_2 and N_2, D_{O_2,N_2}	2.2×10^{-5} m^2/s
Binary diffusivity of N_2 and water vapour,D_{N_2,H_2O}	3.87×10^{-5} m^2/s
Binary diffusivity of H_2 and water vapour,D_{H_2,H_2O}	9.29×10^{-5} m^2/s
Anode charge transfer coefficient,α_a	0.5
Cathode charge transfer coefficient,α_c	0.6
Electrochemical active area of Pt particles,A_{Pt}	40000 m^2/kg
Ref. exchange current density at anode,$i_{o,a}$	3.5×10^3 A/m^2
Ref. exchange current density at cathode,$i_{o,c}$	3×10^{-3} A/m^2
Ref. H_2 concentration,$C_{H_2,ref}$	56.4 mol/m^3
Ref. O_2 concentration,$C_{O,ref}$	0.85111 mol/m^3
Henry's constant of O_2, H_{O_2}	31664 Pa.m^3/mol
Henry's constant of H_2, H_{H_2}	4560 Pa.m^3/mol
Cell active area,A_{act}	9.0×10^{-3} m^2
Membrane thickness,δ_{mem}	5.1×10^{-5} m
Anode/Cathode GDL thickness,δ_{gdl}	1.8×10^{-4} m
Anode/Cathode CL thickness,δ_{cl}	1.0×10^{-5} m
Anode/Cathode GDL porosity,ε_{gdl}	0.70
Anode/Cathode CL porosity,ε_{cl}	0.48
Platinum loading,m_{Pt}	0.01 kg/m^2
GDL thermal conductivity,k_{gdl}	1 W/(m.K)
Membrane thermal conductivity,k_{mem}	0.17 W/(m.K)
Agglomerate radius,r_{agg}	1.0×10^{-7} m

$$a = \frac{P_{\text{H}_2\text{O}}}{P_{\text{sat}}} \tag{25}$$

where $P_{\text{H}_2\text{O}}$ is the partial pressure of water vapour and P_{sat} is the saturation pressure of water vapour which is defined as:

$$\log_{10}P_{\text{sat}} = -2.1794 + 0.02953(T - 273.15) - 9.1837 \times 10^{-5}(T - 273.15)^2 + 1.4454 \times 10^{-7}(T - 273.15)^3 \tag{26}$$

To solve the conservations equations (1)–(5), we need to prescribe appropriate boundary conditions. For the solid-phase potential, cell potential was prescribed at the outermost boundary of the cathode GDL, and zero potential was set for the outermost boundary of the anode GDL. For the membrane phase potential, zero-fluxes were prescribed for the outermost boundaries of the CLs. The boundary temperature at the outermost boundary of the cathode/anode GDL, T_{GDL}, is obtained using the following equation:

$$T_{\text{GDL}} = \begin{cases} \frac{q}{h} + T_\infty \text{for air-breathing PEMFC} \\ \frac{q}{h} + T_{\text{channel}} \text{for conventional PEMFC} \end{cases} \tag{27}$$

where T_∞ and T_{channel} are respectively the ambient temperature and channel temperature, q is the heat flux (computed by the model) and h is the heat transfer coefficient which is the sum of the radiative heat transfer coefficient, h_{rad} , and the convective heat transfer coefficient, h_{conv} :

$$h_{\text{rad}} = 2e\sigma_{\text{Bolt}}\left(T_{GDL}^2 + T_\infty^2\right)(T_{GDL} + T_\infty) \tag{28}$$

$$h_{\text{conv}} = \frac{Nu.k_{\text{air}}}{L_{\text{ch}}} \tag{29}$$

where e is the emissivity, σ_{Bolt} is the Stephan-Boltzmann constant, k_{air} is the air thermal conductivity and L_{ch} is the characteristic length which is 7 cm for air-breathing PEMFC [55] and 1 mm (the side length of the square channel) for conventional PEMFC [11]. Nu is the Nusselt number and is given by:

$$Nu = \begin{cases} 0.16Ra^{1/3}, \text{for air-breathing PEMFC} \\ 3.61, \text{for conventional PEMFC} \end{cases} \tag{30}$$

Note that the expression for Nu for air-breathing PEMFC is that of horizontally-oriented *iso*-flux heated plate [11]. Ra is the Rayleigh number and is given by:

$$Ra = \frac{g\beta q L_{ch}^4}{\nu_{\text{air}}\ \alpha_{\text{air}}\ k_{\text{air}}} \tag{31}$$

where ν_{air} and α_{air} are the kinematic viscosity and thermal diffusivity of air, respectively. β is the thermal expansion coefficient and is obtained by:

$$\beta = \frac{1}{T_f} \tag{32}$$

where T_f is the film temperature and is the mean of the ambient temperature (T_∞) and the temperature of the outer surface of the GDL (T_{GDL}). Likewise, the boundary concentrations of the chemical species, $C_{i,GDL}$, are obtained using the following equation:

$$C_{i,GDL} = \begin{cases} \frac{N_i}{h_{m,i}} + C_{i,\infty} \text{for air-breathing PEMFC} \\ \frac{N_i}{h_{m,i}} + C_{i,channel} \text{for conventional PEMFC} \end{cases} \tag{33}$$

where N_i is the molar flux of the species i (computed by the model), $C_{i,\infty}$ and $C_{i,channel}$ are the molar concentrations of the species i in the ambient and the channel, respectively. $h_{m,i}$ is the mass transfer coefficient and is given by:

$$h_{m,i} = \frac{Sh_i \cdot D_{ij}}{L_{ch,m}} \tag{34}$$

where $L_{ch,m}$ is the characteristic length associated with mass transfer and it corresponds to the side length of the square channel for the conventional PEMFC (1 mm) and the side length of the active area for an air-breathing PEMFC (3 cm) [11]. Sh_i is the Sherwood number of the species i and is determined using the analogy between heat and mass transfer as follows:

$$Sh_i = \begin{cases} 0.16Ra_{m,i}^{1/3}\ , \text{ for air-breathing PEMFC} \\ 3.61\quad , \text{ for conventional PEMFC} \end{cases} \tag{35}$$

$Ra_{m,i}$ is the Rayleigh number associated with mass transfer for the species i and is given by [11]:

$$Ra_{m,i} = \frac{g\gamma\left(x_i^\infty - x_i\right)L_{ch,m}^3}{\nu_i D_{ij}} \tag{36}$$

where g is the acceleration due to gravity, x_i^∞ is the mole fraction of the species i in the ambient region, x_i is the mole fraction of the species i at the surface of the GDL, ν_i is the kinematic viscosity of the species i, and γ is the volumetric expansion coefficient which is given as follows:

$$\gamma = \frac{M_{\text{O}_2} - M_{\text{H}_2\text{O}}}{M_{\text{mix}}} \tag{37}$$

where M_{O_2} and M_{H_2O} are the molecular weights of oxygen and water,

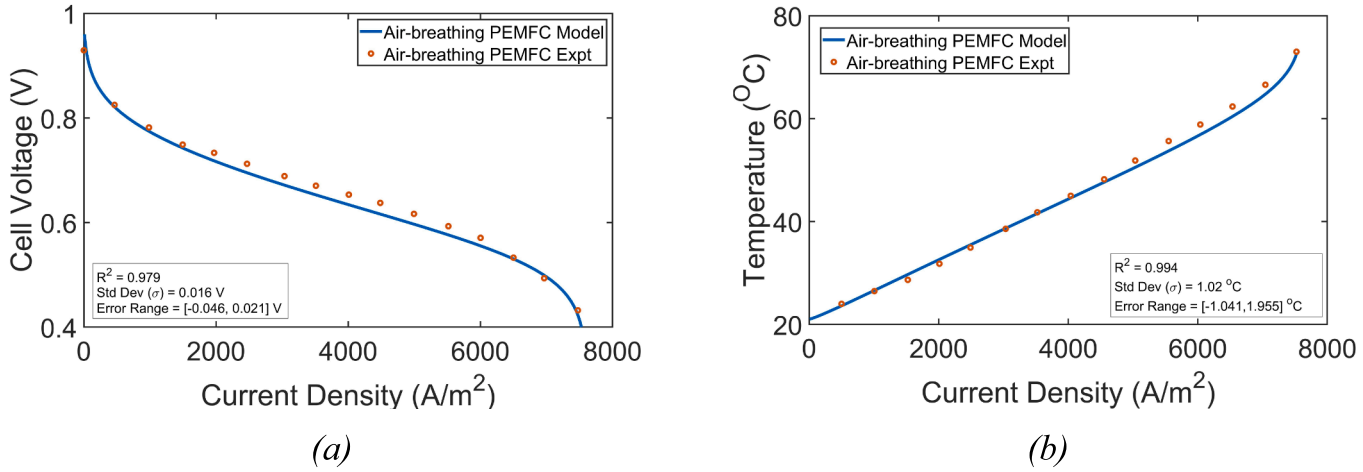

Fig. 3. The modelled and experimental (a) polarization curve and (b) the surface temperature profile of the cathode GDL for an air-breathing PEMFC. The cell temperature is 21 °C and relative humidity is 50 %.

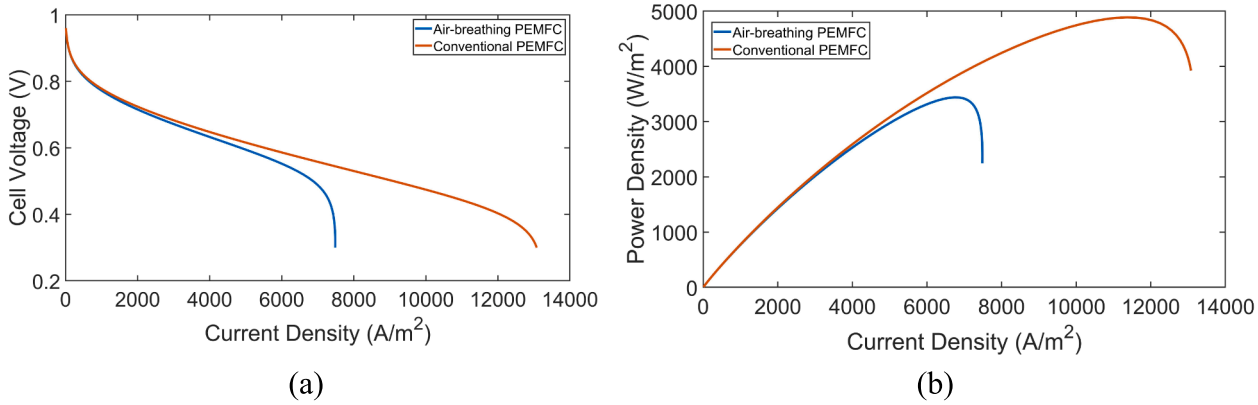

Fig. 4. (a) Polarization and (b) power density curves for the modelled conventional and air-breathing PEMFCs. The cell temperature is 21$^\circ C$ and relative humidity is 50 %.

respectively. M_{mix} is the molecular weight of the binary mixture:

$$M_{\text{mix}} = \frac{M^{\infty}_{\text{mix}} + M^{\text{gdl}}_{\text{mix}}}{2} \tag{38}$$

$$M^{\infty}_{\text{mix}} = \frac{C^{\infty}_{\text{O}_2}}{C^{\infty}_{\text{O}_2} + C^{\infty}_{\text{H}_2\text{O}}} M_{\text{O}_2} + \frac{C^{\infty}_{\text{H}_2\text{O}}}{C^{\infty}_{\text{O}_2} + C^{\infty}_{\text{H}_2\text{O}}} M_{\text{H}_2\text{O}} \tag{39}$$

$C^{\infty}_{\text{O}_2}$ is molar concentration of oxygen in the ambient region and is obtained by:

$$C^{\infty}_{\text{O}_2} = 0.21\left(C^{\infty}_{\text{tot}} - C^{\infty}_{\text{H}_2\text{O}}\right) \tag{40}$$

$C^{\infty}_{H_2O}$ is the molar concentration of water in the ambient air and is given by:

$$C^{\infty}_{H_2\text{O}} = \frac{P_{\infty} \cdot RH}{RT_{\infty}} \tag{41}$$

where RH represents the water relative humidity of the ambient. The molar concentration of ambient air (C^{∞}_{tot}) is determined using the Ideal Gas Law:

$$C^{\infty}_{tot} = \frac{P}{RT_{\infty}} \tag{42}$$

The entire domain was discretized and refined at all the interfaces to ensure obtaining mesh-independent solutions. The number of elements used was 50. Table 1 shows the parameters used in the model.

3. Result and discussion

3.1. Numerical modelling

In this study, the developed air-breathing PEMFC model is validated with the experimental data reported in Fabian et al. [55]. The simulated polarization curve (Fig. 3a) exhibits strong agreement with the experimental results, accurately capturing the steep decline in both activation and concentration polarization loss regimes. Additionally, the temperature profile as a function of current density (Fig. 3b) aligns well with the experimental data. Key statistical metrics, including the coefficient of determination (R^2), standard deviation (σ), and error range, were incorporated into the comparison plots in Fig. 3a and Fig. 3b, to provide a clear quantitative assessment of the agreement between the experiment and simulation.

Fig. 4 shows the performance curves for both the modeled air-breathing and conventional PEMFCs under operating conditions of 21 °C and 50 % RH. The main distinction between the two polarization curves (Fig. 4a) is that the performance of the modeled air-breathing

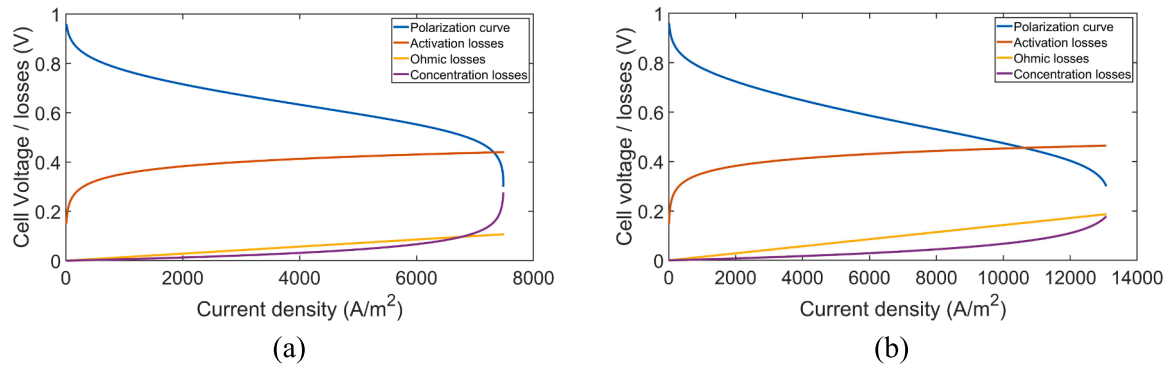

Fig. 5. The various voltages losses as they change with current density for the modelled (a) air-breathing and (b) conventional PEMFCs.

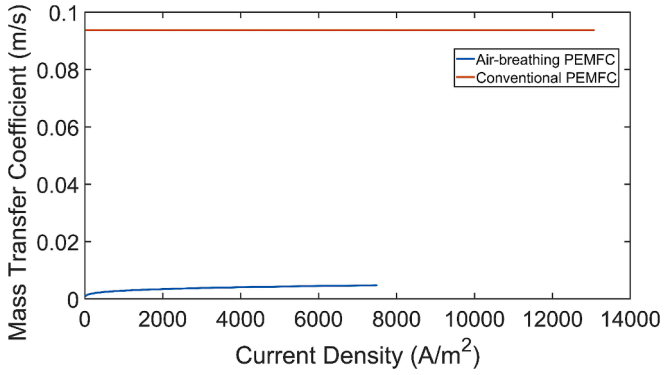

Fig. 6. Mass transfer coefficient as they change with current density for the modelled air-breathing and conventional PEMFCs.

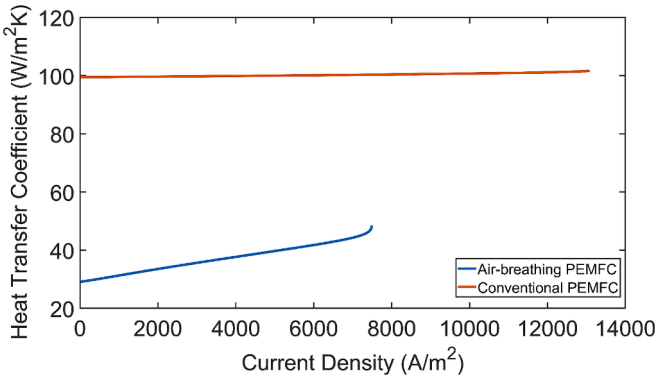

Fig. 8. Heat transfer coefficient as they change with current density for the modelled air-breathing and conventional PEMFCs.

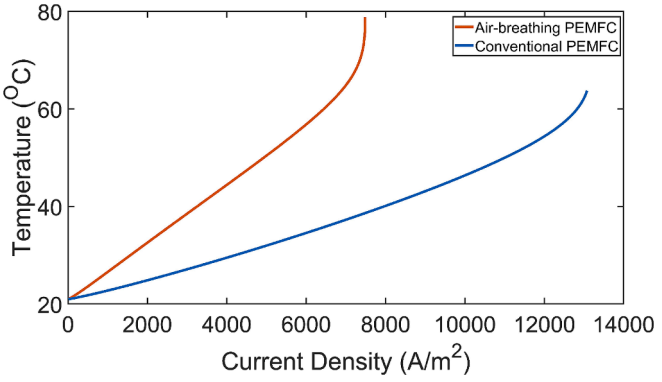

Fig. 7. Cell temperature of the modelled air-breathing and conventional PEMFC as they change with current density.

PEMFC starts to decline sharply at significantly lower current densities compared to the conventional PEMFC. This decline is also mirrored in the power density graphs (Fig. 4b). This decline is attributed to increased concentration losses in the air-breathing PEMFC, as illustrated in Fig. 5. The activation and ohmic losses remain relatively the same in both fuel cell types; however, the concentration losses in the air-breathing PEMFC rise significantly with increasing current. This is primarily due to its significantly lower natural convection-induced mass transfer coefficient for oxygen, which is two orders of magnitude lower than that induced by forced convection (Fig. 6).

The voltage losses convert into waste heat, which raises the cell temperature. Fig. 7 shows how cell temperature changes with current density for both types of fuel cells. Consistent with the polarization curves, the Fig. 7 shows that the temperature of the air-breathing PEMFC increases sharply at significantly lower current densities compared to the conventional PEMFC. This is due to the conventional PEMFC's greater efficiency in dissipating waste heat, which is attributed to its more effective heat transfer mechanisms. Specifically, the heat transfer coefficient for natural convection is an order of magnitude lower than that for forced convection (Fig. 8). Notably, the natural convection-induced heat transfer coefficient increases significantly with current density, as it is also influenced by cell temperature (Equation (5)), which rises significantly with increasing current density.

Unlike zero-dimensional models, the one-dimensional model developed in this study allows for exploring the variation of the key variables across the membrane electrode assembly. Fig. 9 shows the variation in temperature and oxygen molar concentration across the membrane electrode assembly of the fuel cell. In both air-breathing and conventional PEMFCs, the temperature is highest in the cathode catalyst layer as the activation overpotential associated with the oxygen reduction reaction at the cathode CL is the primary source of heat generation. As expected, the temperature profile for the air-breathing PEMFC is significantly higher in comparison to the conventional PEMFC and this is due substantially higher heat transfer coefficient of the former type of fuel cells. Further, the membrane's thermal conductivity is lower than that of the gas diffusion layer, resulting in a steeper temperature gradient across the membrane compared to the GDL. The oxygen concentration decreases from the cathode inlet to the cathode CL, where oxygen is consumed in the reaction. This decrease is more pronounced in the air-breathing PEMFC, as they exhibit a lower mass transfer coefficient, leading to a reduced oxygen concentration at the inlet compared to the conventional PEMFC.

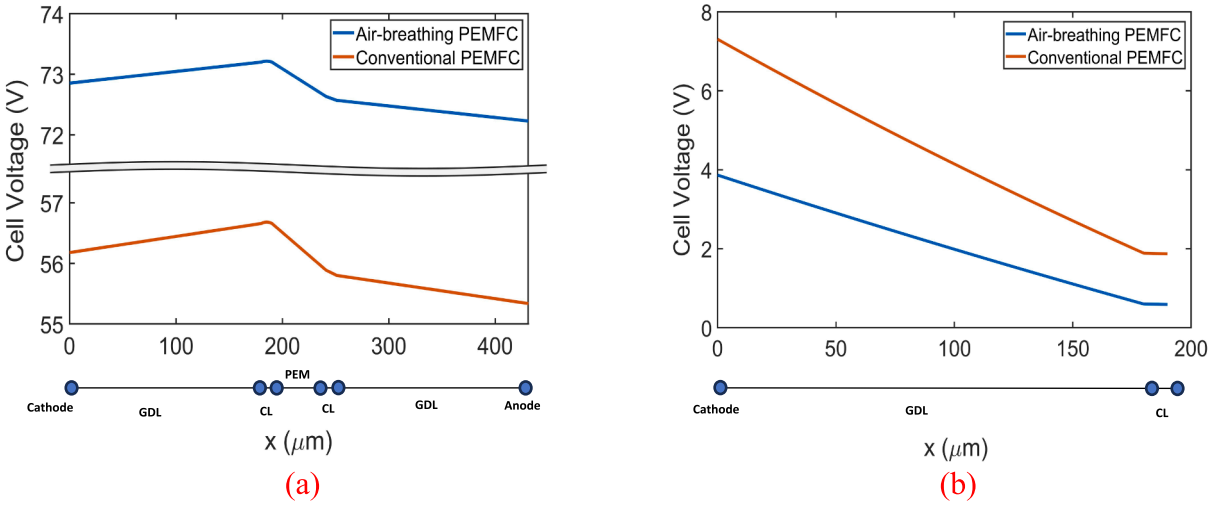

Fig. 9. *The profiles of (a) temperature and (b) molar concentration of oxygen across the modelled air-breathing and conventional PEMFCs.*

Table 2
The factors and levels selected for Taguchi analysis.

Taguchi factors	Level values		
	Low	**Med**	**High**
GDL thickness (μ m)	100	250	400
GDL porosity	0.3	0.5	0.7
GDL electrical conductivity (S/m)	20	60	100
Membrane ionic conductivity (S/m)	2	6	10
CL porosity	0.3	0.5	0.7
Membrane thickness (μ m)	30	50	80

3.2. Taguchi analysis

Taguchi analysis is conducted to identify and rank the most significant parameters or factors affecting both types of fuel cells. Taguchi analysis offers an efficient methodology for identifying key factors and their interactions, guiding experimentation towards performance enhancement at minimal cost [77–80]. In this study, a 6-factor, 3-level design with an L27 orthogonal array and 'larger is better' signal-to-noise (S/N) ratio has been used. A full factorial design with 6 factors and 3 levels, requires 729 experiments, while the L27 array brings this down to just 27 runs.

We have selected what we believe are the six most influential design parameters impacting fuel cell performance and defined their realistic low, medium, and high levels, as shown in Table 2. It should be noted that operational variables such as temperature and relative humidity were not included in the Taguchi analysis. These factors cannot be controlled for air-breathing PEMFCs, which are the focus of this study, as they are influenced by the ambient environment.

The combinations for the 27 runs were generated using MINITAB 16 software, as detailed in Table 3, to construct the L27 orthogonal array.

Table 3
The power density of air-breathing (AB) and conventional (Conv) PEMFCs at 27 combination runs.

No	σ_{GDL} (S/m)	k_{mem} (S/m)	L_{GDL} (μm)	L_{mem} (μm)	ε_{GDL} –	ε_{CL} –	P (W/m^2)	
							AB PEMFC	**Conv. PEMFC**
1	100	0.3	20	2	0.3	30	3019.1	3513.4
2	100	0.3	20	2	0.5	50	2263.8	2495.9
3	100	0.3	20	2	0.7	80	1492.3	1585.8
4	100	0.5	60	6	0.3	30	5749.0	8575.6
5	100	0.5	60	6	0.5	50	4747.4	6228.2
6	100	0.5	60	6	0.7	80	3398.7	4009.9
7	100	0.7	100	10	0.3	30	7480.6	13110.0
8	100	0.7	100	10	0.5	50	6379.6	9517.4
9	100	0.7	100	10	0.7	80	4762.1	6128.2
10	250	0.3	60	10	0.3	50	3067.3	4371.3
11	250	0.3	60	10	0.5	80	2824.1	3876.7
12	250	0.3	60	10	0.7	30	2697.3	3715.3
13	250	0.5	100	2	0.3	50	2929.8	3366.1
14	250	0.5	100	2	0.5	80	2111.5	2300.2
15	250	0.5	100	2	0.7	30	2758.1	3257.3
16	250	0.7	20	6	0.3	50	2971.4	3290.1
17	250	0.7	20	6	0.5	80	2464.8	2681.4
18	250	0.7	20	6	0.7	30	2292.6	2495.9
19	400	0.3	100	6	0.3	80	2254.6	2973.9
20	400	0.3	100	6	0.5	30	2296.7	3110.1
21	400	0.3	100	6	0.7	50	2050.4	2683.5
22	400	0.5	20	10	0.3	80	2202.2	2436.9
23	400	0.5	20	10	0.5	30	2191.9	2438.3
24	400	0.5	20	10	0.7	50	1831.3	1997.8
25	400	0.7	60	2	0.3	80	2060.8	2209.0
26	400	0.7	60	2	0.5	30	2827.4	3181.8
27	400	0.7	60	2	0.7	50	1983.7	2147.8

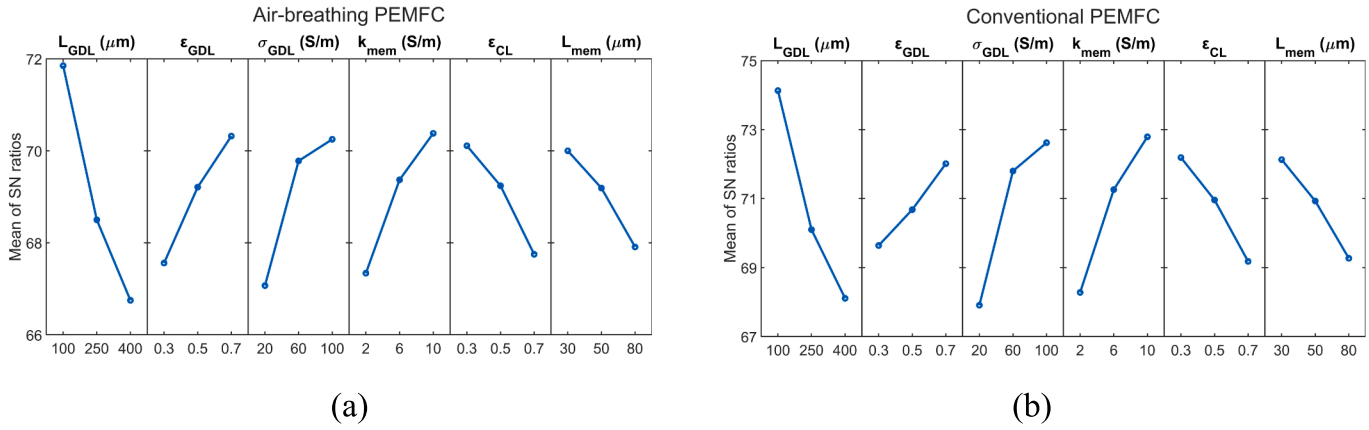

Fig. 10. S/N ratio of different Taguchi factors at different levels for (a) air-breathing and (b) conventional PEMFCs.

Table 4
S/N ratio for different levels of each investigated factor and the ranking of factors based on their influence, as determined by the difference in S/N ratios.

Taguchi factors	Air-breathing PEMFC					Conventional PEMFC				
	Levels			Delta	Rank	Levels			Delta	Rank
	Low	Med	High			Low	Med	High		
L_{GDL}(μm)	71.85	68.5	66.75	5.1	1	74.13	70.1	68.11	6.02	1
ϵ_{GDL}	67.56	69.21	70.32	2.76	4	69.64	70.68	72.01	2.37	6
σ_{GDL}(S/m)	67.07	69.78	70.25	3.19	2	67.91	71.8	72.62	4.71	2
k_{mem}(S/m)	67.34	69.37	70.38	3.04	3	68.28	71.26	72.79	4.52	3
ϵ_{CL}	70.11	69.24	67.75	2.36	5	72.19	70.96	69.18	3.01	4
L_{PEM}(μ m)	70	69.19	67.91	2.09	6	72.13	70.93	69.27	2.86	5

Table 5
Selection of factors and levels for the Taguchi analysis.

Taguchi factors	Level values		
	Low	Med	High
GDL thickness (μ m)	100	120	140
GDL porosity	0.5	0.6	0.7
GDL electrical conductivity (S/m)	80	90	100
Membrane ionic conductivity (S/m)	6	8	10
CL porosity	0.3	0.4	0.5
Membrane thickness (μ m)	30	40	50

Following this, the maximum power density for each run was calculated from simulating the modelled fuel cells, and these are used for the Taguchi analysis. The goal of the Taguchi analysis in this case is to optimize the levels of each factor to maximize power output. It should be noted that the maximum power density in the air-breathing PEMFC is consistently lower than that of the conventional type.

Fig. 10 and Table 4 illustrate the effect of each factor level on the mean S/N ratio for both air-breathing and conventional PEMFCs. Here, the "signal" represents the magnitude of the desired outcome (i.e., output power density), while the "noise" represents the undesirable variation in the output due to variability in the factors. Thus, higher S/N ratios indicate both stronger performance and less variability.

Higher S/N ratio in this case corresponds to more favorable outcome (higher output power in this study) because 'larger is better' S/N ratio technique is employed in this study. Taguchi analysis also provides an overall trend of the output power with variations in values of different parameters. For example, the S/N ratio increases with increasing porosity and electrical conductivity of cathode GDL for both the types of PEMFC, and hence it means that the PEMFC performs better at higher values of these factors.

The significance order of parameters in Taguchi analysis depends on the range of levels chosen for each factor. Thus, the ranking does not definitively indicate that one factor is more significant than another. However, it serves to reveal whether both fuel cell types exhibit similar sensitivity to the selected parameters. Examination of Table 4 reveals consistent behavior across both fuel cell types with variations in different parameters. The analysis shows that the thickness of the gas diffusion layer appears to be the most influential factor for both air-breathing and conventional PEMFCs. Additionally, membrane conductivity and gas diffusion layer conductivity are key influential factors. However, the conventional PEMFC shows a greater sensitivity to these parameters as it could be inferred from the higher delta values. GDL porosity has a high significance for the air-breathing PEMFC because an

Table 6
Comparison of optimized power output from Taguchi analysis and numerical model for air-breathing (AB) and conventional (Conv.) PEMFCs across different parameter ranges.

Type of PEMFC	Range of levels	Optimized power (W/m^2) from		Percentage deviation
		Taguchi analysis	Numerical model	
AB PEMFC	wide	7717	7481	3.16 %
	narrow	7512	7481	0.43 %
Conv. PEMFC	wide	12566	13110	4.15 %
	narrow	13059	13110	0.39 %

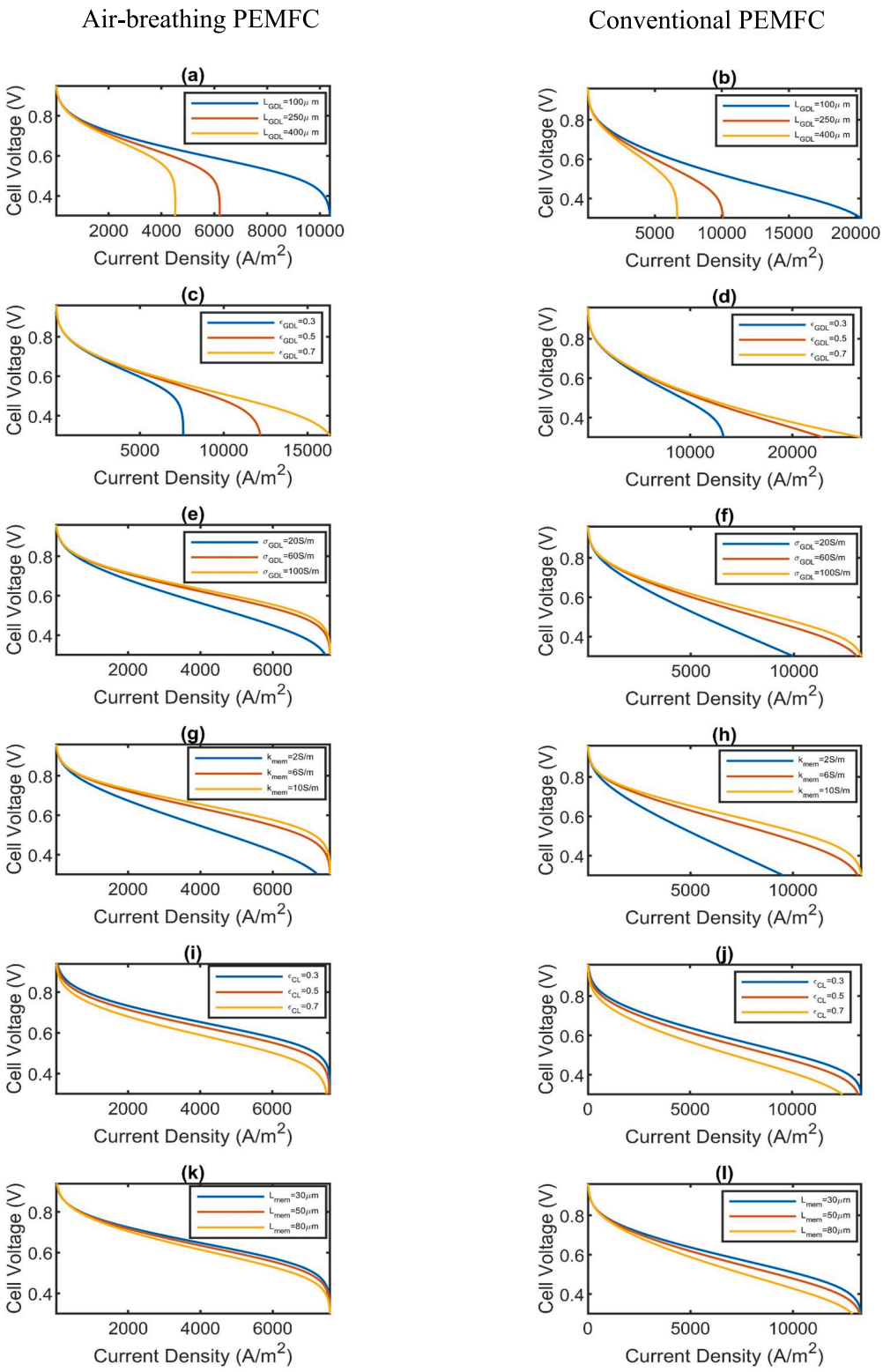

Fig. 11. Comparative parametric analysis of air-breathing and conventional PEMFCs: left column depicts air-breathing PEMFCs, and right column depicts conventional PEMFCs.

increase in its value can significantly decrease the mass transfer resistance and thus increase the cell performance. This explains the relatively higher rank of GDL porosity for the air-breathing PEMFC compared to the conventional PEMFC.

To validate the results obtained by Taguchi Analysis, a comparison with the result from the numerical model was conducted. The maximum output power density could be obtained using the following equation [80]

$$\gamma_{opt} = -10\log_{10}\left(\frac{1}{P^2_{max}}\right) \tag{43}$$

where γ_{opt} represents the optimized S/N ratio corresponding to the maximum power (P_{max}), and is given by

$$\gamma_{opt} = \gamma + \sum_{i=1}^{9} \Delta F_i \quad (44)$$

where γ is the overall mean of all the S/N ratios of a particular type of PEMFC, and ΔF_i is the difference of the overall S/N ratio mean and the mean S/N ratio of the optimal level (i.e, highest value) of factor F_i. In this case, γ_{opt} could be determined as

$$\gamma_{opt} = \gamma + \Delta(\sigma_{GDL}) + \Delta(k_{mem}) + \Delta(L_{GDL}) + \Delta(L_{mem}) + \Delta(\varepsilon_{GDL}) + \Delta(\varepsilon_{CL}) \quad (45)$$

The value of P_{max} obtained from the above equations was compared with the optimal power predicted by the numerical models. The analysis revealed deviations of approximately 3.16 % for the air-breathing PEMFC and 4.15 % for the conventional PEMFC; see Table 5. These deviations are relatively acceptable; however, the accuracy of predictions of Taguchi analysis could be improved with narrower level ranges as shown in Table 5. The accuracy of the Taguchi analysis improved significantly, with deviations reduced to just 0.43 % for the air-breathing PEMFC and 0.39 % for the conventional PEMFC (Table 6).

3.3. Parametric analysis

To evaluate the sensitivity of fuel cell performance to the factors investigated in the Taguchi analysis, a parametric study was conducted employing the model created for each fuel cell type. This study tested each factor across a broader range of realistic levels to better understand their effects on fuel cell performance. Fig. 11 shows the polarization curves for each factor at various levels for each fuel cell type. The figure confirms that the sensitivity of fuel cell performance to the investigated factors generally aligns with the rankings proposed by the Taguchi analysis (Table 4). Specifically, both types of fuel cells show the greatest sensitivity to GDL thickness (ranked highest in the Taguchi analysis) and the least sensitivity to membrane thickness (ranked lowest for the air-breathing PEMFC and fifth for the conventional PEMFC in the Taguchi analysis).

Optimizing GDL thickness is crucial for balancing performance factors in PEMFCs. Increased thickness enhances water retention, aiding membrane hydration and sustaining proton conductivity, but also raises mass transport resistance, potentially impeding reactant gas diffusion and affecting long-term performance. Striking this balance is key to effective GDL design for practical applications.

Several key observations are highlighted. Reducing cathode GDL thickness and increasing its porosity notably improves the performance of both fuel cell types. However, the air-breathing PEMFC is significantly more sensitive to an increase in GDL porosity from 0.5 to 0.7 compared to the conventional PEMFC. This increased sensitivity is due to the air-breathing PEMFC being more diffusion-limited, particularly at high current densities, because of the lower mass transport coefficient of oxygen. Increased GDL porosity enhances oxygen diffusivity and reduces mass transport resistance in the air-breathing PEMFC. On the other hand, for the conventional PEMFC, increasing GDL porosity from 0.5 to 0.7 provides minimal performance gain, as it is near its maximum diffusive capacity. One more observation is that, for both types of fuel cells, the electrical conductivity of the GDL and the ionic conductivity of the membrane have a limited impact on performance beyond certain values. Specifically, increasing the GDL electrical conductivity from 60 to 100 S/m and the membrane ionic conductivity from 6 to 10 S/m results in only marginal improvements in fuel cell performance. Finally, the performance of both types of PEMFCs is significantly less sensitive to the porosity of the CL compared to the porosity of the GDL. This is because the CL is an order of magnitude thinner than the GDL, and oxygen begins to react as soon as it enters the CL.

4. Summary and Conclusions

Comprehensive one-dimensional models for air-breathing and conventional PEMFCs have been developed to evaluate the sensitivity of fuel cell performance to key design parameters. Taguchi analysis was used to rank these parameters based on their impact. This novel approach, combining numerical modelling with Taguchi analysis, provides valuable insights for optimizing air-breathing PEMFCs, which are promising for powering small electronic devices. The key findings are as follows:

- The air-breathing PEMFC exhibits a sharp decline in performance at lower current densities compared to the conventional PEMFC. This decline is due to increased concentration losses in the air-breathing PEMFC and is attributed to its much lower natural convection-induced mass transfer coefficient for oxygen.
- The temperature of the air-breathing PEMFC rises sharply at lower current densities than the conventional PEMFC, due to less effective heat dissipation. This is linked to the lower natural convection heat transfer coefficient compared to forced convection.
- The parametric study using fuel cell models generally confirms that performance sensitivity to the tested factors matches the Taguchi analysis rankings. Both air-breathing and conventional PEMFCs are most sensitive to GDL thickness and least sensitive to membrane thickness, consistent with the Taguchi analysis results.
- The maximum power density obtained from the Taguchi calculations was in excellent agreement with the values obtained from the numerical models for both types of fuel cells.
- Reducing cathode GDL thickness and increasing its porosity significantly improve the performance of both fuel cell types. However, the air-breathing PEMFC shows greater sensitivity to increasing GDL porosity from 0.5 to 0.7, and this is due to its higher diffusion limitation and lower oxygen mass transport coefficient induced by natural convection compared to the conventional PEMFC.
- Electrical conductivity of the GDL and ionic conductivity of the membrane have limited impact on fuel cell performance beyond certain values. Specifically, increasing GDL electrical conductivity from 60 to 100 S/m and membrane ionic conductivity from 6 to 10 S/m results in only marginal performance improvements.
- Performance sensitivity to CL porosity is notably less compared to GDL porosity for both fuel cell types. This is because the CL is much thinner than the GDL, and oxygen starts to react immediately upon entering the CL.

CRediT authorship contribution statement

Faseeh Abdulrahman: Writing – review & editing, Writing – original draft, Visualization, Validation, Software, Formal analysis, Data curation, Conceptualization. **Mohammed S. Ismail:** Writing – review & editing, Writing – original draft, Visualization, Supervision, Methodology, Investigation, Formal analysis, Conceptualization. **S. Mani Sarathy:** Writing – review & editing, Supervision, Resources, Project administration, Funding acquisition, Conceptualization.

Declaration of competing interest

The authors declare that they have no known competing financial interests or personal relationships that could have appeared to influence the work reported in this paper.

Acknowledgements

This work was supported by the KAUST FLEET consortium and its member companies.

Data availability

Data will be made available on request.

References

[1] International Energy Outlook: US Energy Information Administration; 202Available from: https://www.eia.gov/outlooks/ieo/consumption/sub-topic-03.php.

[2] Global Energy Perspective 2023: Power outlook: McKinsey & Company, MC; 2023 [updated January 16, 2024]. Available from: https://www.mckinsey.com/industries/oil-and-gas/our-insights/global-energy-perspective-2023-power-outlook.

[3] Edwards PP, Kuznetsov VL, David WIF, Brandon NP. Hydrogen and fuel cells: towards a sustainable energy future. Energy Policy 2008;36(12):4356–62. https://doi.org/10.1016/j.enpol.2008.09.036.

[4] Singla MK, Nijhawan P, Oberoi AS. Hydrogen fuel and fuel cell technology for cleaner future: a review. Environ Sci Pollut Res Int 2021;28(13):15607–26. https://doi.org/10.1007/s11356-020-12231-8.

[5] Felseghi R-A, Carcadea E, Raboaca MS, Trufin CN, Filote C. Hydrogen fuel cell technology for the sustainable future of stationary applications. Energies 2019;12(23). https://doi.org/10.3390/en12234593.

[6] Hwang J-J. Sustainability study of hydrogen pathways for fuel cell vehicle applications. Renew Sustain Energy Rev 2013;19:220–9. https://doi.org/10.1016/j.rser.2012.11.033.

[7] Sun D, Liu Z. Performance and economic study of a novel high-efficiency PEMFC vehicle thermal management system applied for cold conditions. Energy 2024;305. https://doi.org/10.1016/j.energy.2024.132415.

[8] Guerrero Moreno N, Cisneros Molina M, Gervasio D, Pérez Robles JF. Approaches to polymer electrolyte membrane fuel cells (PEMFCs) and their cost. Renew Sustain Energy Rev 2015;52:897–906. https://doi.org/10.1016/j.rser.2015.07.157.

[9] Alharbi AG, Olabi AG, Rezk H, Fathy A, Abdelkareem MA. Optimized energy management and control strategy of photovoltaic/PEM fuel cell/batteries/supercapacitors DC microgrid system. Energy 2024;290. https://doi.org/10.1016/j.energy.2023.130121.

[10] Sapkota P, Boyer C, Dutta R, Cazorla C, Aguey-Zinsou K-F. Planar polymer electrolyte membrane fuel cells: powering portable devices from hydrogen. Sustainable Energy Fuels 2020;4(2):439–68. https://doi.org/10.1039/c9se00861f.

[11] Calili-Cankir F, Ismail MS, Ingham DB, Hughes KJ, Ma L, Pourkashanian M. Air-breathing versus conventional polymer electrolyte fuel cells: a parametric numerical study. Energy 2022;250. https://doi.org/10.1016/j.energy.2022.123827.

[12] Fly A, Thring RH. A comparison of evaporative and liquid cooling methods for fuel cell vehicles. Int J Hydrogen Energy 2016;41(32):14217–29. https://doi.org/10.1016/j.ijhydene.2016.06.089.

[13] Saygili Y, Eroglu I, Kincal S. Model based temperature controller development for water cooled PEM fuel cell systems. Int J Hydrogen Energy 2015;40(1):615–22. https://doi.org/10.1016/j.ijhydene.2014.10.047.

[14] Wang Y, Liu B, Li Q, Cartmell S, Ferrara S, Deng ZD, et al. Lithium and lithium ion batteries for applications in microelectronic devices: a review. J Power Sources 2015;286:330–45. https://doi.org/10.1016/j.jpowsour.2015.03.164.

[15] Şen M, Özcan M, Eker YR. A review on the lithium-ion battery problems used in electric vehicles. Next Sustainability 2024;3. https://doi.org/10.1016/j.nxsust.2024.100036.

[16] Zuo W, Zhang Y, Jiaqiang E, Li J, Li Q, Zhang G. Performance comparison between single S-channel and double S-channel cold plate for thermal management of a prismatic LiFePO4 battery. Renew Energy 2022;192:46–57. https://doi.org/10.1016/j.renene.2022.04.116.

[17] Li F, Zuo W, Zhou K, Li Q, Huang Y. State of charge estimation of lithium-ion batteries based on PSO-TCN-Attention neural network. J Storage Mater 2024;84. https://doi.org/10.1016/j.est.2024.110806.

[18] Liu Z, Sun T, Bai F. Numerical study on effect of flow field configuration on air-breathing proton exchange membrane fuel stacks. Energies 2024;17(11). https://doi.org/10.3390/en17112501.

[19] Calili-Cankir F, Ismail MS, Ingham DB, Hughes KJ, Ma L, Pourkashanian M. Air-breathing polymer electrolyte fuel cells: a review. Renew Energy 2023;213:86–108. https://doi.org/10.1016/j.renene.2023.05.134.

[20] Guida D, Minutillo M. Design methodology for a PEM fuel cell power system in a more electrical aircraft. Appl Energy 2017;192:446–56. https://doi.org/10.1016/j.apenergy.2016.10.090.

[21] Wang Y, Seo B, Wang B, Zamel N, Jiao K, Adroher XC. Fundamentals, materials, and machine learning of polymer electrolyte membrane fuel cell technology. Energy AI 2020;1. https://doi.org/10.1016/j.egyai.2020.100014.

[22] Shyu JC, Setiyo M, Marliyati M, Apriandi N, Margana M, Sulistiyo W, et al. Application of a PEM fuel cell engine as a small-scale power generator for small cars with different fuel concentrations. Automotive Experiences 2023;6(2):273–89. https://doi.org/10.31603/ae.9225.

[23] Tohidi M, Mansouri SH, Amiri H. Effect of primary parameters on the performance of PEM fuel cell. Int J Hydrogen Energy 2010;35(17):9338–48. https://doi.org/10.1016/j.ijhydene.2010.03.112.

[24] Carcadea E, Varlam M, Ismail M, Ingham DB, Marinoiu A, Raceanu M, et al. PEM fuel cell performance improvement through numerical optimization of the parameters of the porous layers. Int J Hydrogen Energy 2020;45(14):7968–80. https://doi.org/10.1016/j.ijhydene.2019.08.219.

[25] Carton JG, Olabi AG. Three-dimensional proton exchange membrane fuel cell model: comparison of double channel and open pore cellular foam flow plates. Energy 2017;136:185–95. https://doi.org/10.1016/j.energy.2016.02.010.

[26] Huang T, Dingxun Y, Ren X, Ma J, Chen X, Ou C, et al. Effect of operating conditions of unmanned aerial vehicle powered by PEMFC on water and heat distributions of cell. Int J Green Energy 2023;21(8):1815–28. https://doi.org/10.1080/15435075.2023.2272847.

[27] Hazar H, Yilmaz M, Sevinc H. A comparative analysis of a novel flow field pattern with different channel size configurations. Fuel 2022;319. https://doi.org/10.1016/j.fuel.2022.123867.

[28] Um S, Wang C-Y. Computational study of water transport in proton exchange membrane fuel cells. J Power Sources 2006;156(2):211–23. https://doi.org/10.1016/j.jpowsour.2005.05.095.

[29] Falcão DS, Oliveira VB, Rangel CM, Pinho C, Pinto AMFR. Water transport through a PEM fuel cell: a one-dimensional model with heat transfer effects. Chem Eng Sci 2009;64(9):2216–25. https://doi.org/10.1016/j.ces.2009.01.049.

[30] Janssen GJM, Overvelde MLJ. Water transport in the proton-exchange-membrane fuel cell: measurements of the effective drag coefficient. J Power Sources 2001;101(1):117–25. https://doi.org/10.1016/s0378-7753(01)00708-x.

[31] Yan Q, Toghiani H, Causey H. Steady state and dynamic performance of proton exchange membrane fuel cells (PEMFCs) under various operating conditions and load changes. J Power Sources 2006;161(1):492–502. https://doi.org/10.1016/j.jpowsour.2006.03.077.

[32] Mann RF, Amphlett JC, Hooper MAI, Jensen HM, Peppley BA, Roberge PR. Development and application of a generalised steady-state electrochemical model for a PEM fuel cell. J Power Sources 2000;86(1–2):173–80. https://doi.org/10.1016/s0378-7753(99)00484-x.

[33] Ge S-H, Yi B-L. A mathematical model for PEMFC in different flow modes. J Power Sources 2003;124(1):1–11. https://doi.org/10.1016/s0378-7753(03)00584-6.

[34] Matamoros L, Brüggemann D. Concentration and ohmic losses in free-breathing PEMFC. J Power Sources 2007;173(1):367–74. https://doi.org/10.1016/j.jpowsour.2007.02.091.

[35] Manoj Kumar P, Kolar AK. Effect of cathode channel dimensions on the performance of an air-breathing PEM fuel cell. Int J Therm Sci 2010;49(5):844–57. https://doi.org/10.1016/j.ijthermalsci.2009.12.002.

[36] Jeong SU, Cho EA, Kim H-J, Lim T-H, Oh I-H, Kim SH. A study on cathode structure and water transport in air-breathing PEM fuel cells. J Power Sources 2006;159(2):1089–94. https://doi.org/10.1016/j.jpowsour.2005.12.046.

[37] Husar A, Strahl S, Riera J. Experimental characterization methodology for the identification of voltage losses of PEMFC: applied to an open cathode stack. Int J Hydrogen Energy 2012;37(8):7309–15. https://doi.org/10.1016/j.ijhydene.2011.11.130.

[38] Manoj Kumar P, Parthasarathy V. A passive method of water management for an air-breathing proton exchange membrane fuel cell. Energy 2013;51:457–61. https://doi.org/10.1016/j.energy.2012.12.015.

[39] Yu XX, Liu Y, Tu ZK, Chan SH. Endplate effect in an open-cathode proton exchange membrane fuel cell stack: phenomenon and resolution. Renew Energy 2023;219. https://doi.org/10.1016/j.renene.2023.119392.

[40] Ismail MS, Ingham DB, Hughes KJ, Ma L, Pourkashanian M. Thermal modelling of the cathode in air-breathing PEM fuel cells. Appl Energy 2013;111:529–37. https://doi.org/10.1016/j.apenergy.2013.05.007.

[41] Zhang Y, Pitchumani R. Numerical studies on an air-breathing proton exchange membrane (PEM) fuel cell. Int J Heat Mass Transf 2007;50(23–24):4698–712. https://doi.org/10.1016/j.ijheatmasstransfer.2007.03.044.

[42] Zhang Y, Mawardi A, Pitchumani R. Numerical studies on an air-breathing proton exchange membrane (PEM) fuel cell stack. J Power Sources 2007;173(1):264–76. https://doi.org/10.1016/j.jpowsour.2007.05.008.

[43] Hwang JJ. Species-electrochemical modeling of an air-breathing cathode of a planar fuel cell. Journal of The Electrochemical Society 2006;153(8). https://doi.org/10.1149/1.2209567.

[44] Wang Y, Ouyang M. Three-dimensional heat and mass transfer analysis in an air-breathing proton exchange membrane fuel cell. J Power Sources 2007;164(2):721–9. https://doi.org/10.1016/j.jpowsour.2006.11.056.

[45] Manoj Kumar P, Kolar AK. Effect of cathode design on the performance of an air-breathing PEM fuel cell. Int J Hydrogen Energy 2010;35(2):671–81. https://doi.org/10.1016/j.ijhydene.2009.10.086.

[46] Calili F, Ismail MS, Ingham DB, Hughes KJ, Ma L, Pourkashanian M. A dynamic model of air-breathing polymer electrolyte fuel cell (PEFC): a parametric study. Int J Hydrogen Energy 2021;46(33):17343–57. https://doi.org/10.1016/j.ijhydene.2021.02.133.

[47] Calili-Cankir F, Ismail MS, Berber MR, Alrowaili ZA, Ingham DB, Hughes KJ, et al. Dynamic models for air-breathing and conventional polymer electrolyte fuel cells: a comparative study. Renew Energy 2022;195:1001–14. https://doi.org/10.1016/j.renene.2022.06.092.

[48] Yalcinoz T, Alam MS. Dynamic modeling and simulation of air-breathing proton exchange membrane fuel cell. J Power Sources 2008;182(1):168–74. https://doi.org/10.1016/j.jpowsour.2008.03.076.

[49] Schmitz A, Ziegler C, Schumacher JO, Tranitz M, Fontes E, Hebling C. Modelling approach for planar self-breathing PEMFC and comparison with experimental results. Fuel Cells 2004;4(4):358–64. https://doi.org/10.1002/fuce.200400034.

[50] Matsuura T, Chen J, Siegel JB, Stefanopoulou AG. Degradation phenomena in PEM fuel cell with dead-ended anode. Int J Hydrogen Energy 2013;38(26):11346–56. https://doi.org/10.1016/j.ijhydene.2013.06.096.

[51] Fan L, Xing L, Tu Z, Hwa CS. A breakthrough hydrogen and oxygen utilization in a H2-O2 PEMFC stack with dead-ended anode and cathode. Energ Conver Manage 2021;243. https://doi.org/10.1016/j.enconman.2021.114404.

[52] Ying W, Ke J, Lee W, Yang T, Kim C. Effects of cathode channel configurations on the performance of an air-breathing PEMFC. Int J Hydrogen Energy 2005;30(12):1351–61. https://doi.org/10.1016/j.ijhydene.2005.04.009.
[53] Ying W, Sohn Y-J, Lee W-Y, Ke J, Kim C-S. Three-dimensional modeling and experimental investigation for an air-breathing polymer electrolyte membrane fuel cell (PEMFC). J Power Sources 2005;145(2):563–71. https://doi.org/10.1016/j.jpowsour.2005.01.083.
[54] Ying W, Yang T-H, Lee W-Y, Ke J, Kim C-S. Three-dimensional analysis for effect of channel configuration on the performance of a small air-breathing proton exchange membrane fuel cell (PEMFC). J Power Sources 2005;145(2):572–81. https://doi.org/10.1016/j.jpowsour.2005.02.066.
[55] Fabian T, Posner JD, O'Hayre R, Cha S-W, Eaton JK, Prinz FB, et al. The role of ambient conditions on the performance of a planar, air-breathing hydrogen PEM fuel cell. J Power Sources 2006;161(1):168–82. https://doi.org/10.1016/j.jpowsour.2006.03.054.
[56] Williamson Z, Kim D, Chun D-K, Lee T, Squibb C. Experimental evaluation of cell temperature effects on miniature, air-breathing PEM fuel cells. Appl Therm Eng 2011;31(17–18):3761–7. https://doi.org/10.1016/j.applthermaleng.2011.06.010.
[57] Al-Anazi A, Wilberforce T, Khatib FN, Vichare P, Olabi AG. Performance evaluation of an air breathing polymer electrolyte membrane (PEM) fuel cell in harsh environments – a case study under Saudi Arabia's ambient condition. Int J Hydrogen Energy 2021;46(45):23463–79. https://doi.org/10.1016/j.ijhydene.2020.10.258.
[58] Yan W-M, Zeng M-S, Yang T-F, Chen C-Y, Amani M, Amani P. Performance improvement of air-breathing proton exchange membrane fuel cell stacks by thermal management. Int J Hydrogen Energy 2020;45(42):22324–39. https://doi.org/10.1016/j.ijhydene.2019.08.146.
[59] Henriques T, César B, Branco PJC. Increasing the efficiency of a portable PEM fuel cell by altering the cathode channel geometry: a numerical and experimental study. Appl Energy 2010;87(4):1400–9. https://doi.org/10.1016/j.apenergy.2009.09.001.
[60] Matamoros L, Brüggemann D. Simulation of the water and heat management in proton exchange membrane fuel cells. J Power Sources 2006;161(1):203–13. https://doi.org/10.1016/j.jpowsour.2006.03.078.
[61] Shen J, Tu Z. Flow channel design in a proton exchange membrane fuel cell: From 2D to 3D. Int J Hydrogen Energy 2022;47(5):3087–98. https://doi.org/10.1016/j.ijhydene.2021.10.252.
[62] Chen Z, Zuo W, Zhou K, Li Q, Huang Y, Jiaqiang E. Multi-objective optimization of proton exchange membrane fuel cells by RSM and NSGA-II. Energ Conver Manage 2023;277. https://doi.org/10.1016/j.enconman.2023.116691.
[63] Chen Z, Zuo W, Zhou K, Li Q, Yi Z, Huang Y. Numerical investigation on the performance enhancement of PEMFC with gradient sinusoidal-wave fins in cathode channel. Energy 2024;288. https://doi.org/10.1016/j.energy.2023.129894.
[64] Jeon DH. Effect of gas diffusion layer thickness on liquid water transport characteristics in polymer electrolyte membrane fuel cells. J Power Sources 2020;475. https://doi.org/10.1016/j.jpowsour.2020.228578.
[65] Okonkwo PC, Otor C. A review of gas diffusion layer properties and water management in proton exchange membrane fuel cell system. Int J Energy Res 2020;45(3):3780–800. https://doi.org/10.1002/er.6227.
[66] Ma T, Guo H, Gu Z, Lin W, Qi J, Yu C, et al. Performance analysis and experimental study of titanium GDL in proton exchange membrane fuel cell. Int J Hydrogen Energy 2024;83:604–13. https://doi.org/10.1016/j.ijhydene.2024.08.012.
[67] Ismail MS, Ingham DB, Ma L, Hughes KJ, Pourkashanian M. Effects of catalyst agglomerate shape in polymer electrolyte fuel cells investigated by a multi-scale modelling framework. Energy 2017;122:420–30. https://doi.org/10.1016/j.energy.2017.01.092.
[68] Tian J, Ismail MS, Hughes KJ, Ingham DB, Ma L, Pourkashanian M. Influence of catalyst agglomerate internal structure on PEFC performance investigated by a multiscale numerical model. Fuel 2024;371. https://doi.org/10.1016/j.fuel.2024.131862.
[69] Wu G, Luo N. Multi-objective optimization of PEMFC performance based on grey correlation analysis and response surface method. Front EnergyResearch 2023;11. https://doi.org/10.3389/fenrg.2023.1206418.
[70] Ismail MS, Ingham DB, Hughes KJ, Ma L, Pourkashanian M. An efficient mathematical model for air-breathing PEM fuel cells. Appl Energy 2014;135:490–503. https://doi.org/10.1016/j.apenergy.2014.08.113.
[71] Ismail MS, Ingham DB, Hughes KJ, Ma L, Pourkashanian M. Effective diffusivity of polymer electrolyte fuel cell gas diffusion layers: an overview and numerical study. Int J Hydrogen Energy 2015;40(34):10994–1010. https://doi.org/10.1016/j.ijhydene.2015.06.073.
[72] Zhang X, Yang J, Ma X, Zhuge W, Shuai S. Modelling and analysis on effects of penetration of microporous layer into gas diffusion layer in PEM fuel cells: focusing on mass transport. Energy 2022;254. https://doi.org/10.1016/j.energy.2022.124103.
[73] Moore M, Wardlaw P, Dobson P, Boisvert JJ, Putz A, Spiteri RJ, et al. Understanding the effect of kinetic and mass transport processes in cathode agglomerates. J Electrochem Soc 2014;161(8):E3125–37. https://doi.org/10.1149/2.010408jes.
[74] Kamarajugadda S, Mazumder S. Generalized flooded agglomerate model for the cathode catalyst layer of a polymer electrolyte membrane fuel cell. J Power Sources 2012;208:328–39. https://doi.org/10.1016/j.jpowsour.2012.02.063.
[75] Yoon W, Weber AZ. Modeling low-platinum-loading effects in fuel-cell catalyst layers. Journal of The Electrochemical Society 2011;158(8). https://doi.org/10.1149/1.3597644.
[76] Sun W, Peppley BA, Karan K. An improved two-dimensional agglomerate cathode model to study the influence of catalyst layer structural parameters. Electrochimica Acta 2005;50(16–17):3359–74. https://doi.org/10.1016/j.electacta.2004.12.009.
[77] Zhang Q, Feng J, Zhang Q, Peng X. Performance prediction and evaluation of the scroll-type hydrogen pump for FCVs based on CFD–Taguchi method. Int J Hydrogen Energy 2019;44(29):15333–43. https://doi.org/10.1016/j.ijhydene.2019.04.019.
[78] Amadane Y, Mounir H, El Marjani A, Bouhrim H, Rafi MA. Taguchi approach in combination with CFD simulation as a technique for the optimization of the operating conditions of PEM fuel cells. Arab J Sci Eng 2020;45(9):7587–97. https://doi.org/10.1007/s13369-020-04706-0.
[79] Amadane Y, Mounir H. Performance improvement of a PEMFC with dead-end anode by using CFD-Taguchi approach. J Electroanal Chem 2022;904. https://doi.org/10.1016/j.jelechem.2021.115909.
[80] Karthikeyan P, Muthukumar M, Vignesh Shanmugam S, Pravin Kumar P, Murali S, Senthil Kumar AP. Optimization of operating and design parameters on proton exchange membrane fuel cell by using taguchi method. Procedia Eng 2013;64:409–18. https://doi.org/10.1016/j.proeng.2013.09.114.